



A study of carbon deposition on solid oxide fuel cell anodes using electrochemical impedance spectroscopy in combination with a high temperature crystal microbalance

Jason Millichamp ^a, Thomas J. Mason ^a, Nigel P. Brandon ^b, Richard J.C. Brown ^c, Robert C. Maher ^d, George Manos ^a, Tobias P. Neville ^a, Daniel J.L. Brett ^{a,*}

^a The Centre for CO₂ Technology, Department of Chemical Engineering, UCL, London WC1E 7JE, UK

^b The Energy Futures Lab, Imperial College London, London SW7 2AZ, UK

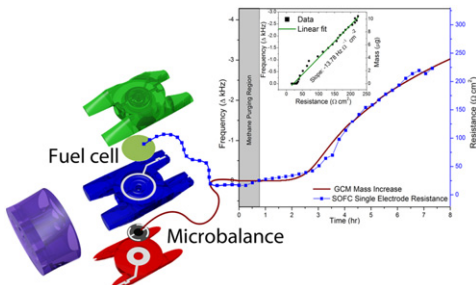
^c Analytical Science Division, National Physical Laboratory, Teddington TW11 0LW, UK

^d The Blackett Laboratory, Prince Consort Road, Imperial College London, London SW7 2BW, UK

HIGHLIGHTS

- A novel sensor is demonstrated to measure carbon deposition on heterogeneous catalyst surfaces.
- Link between carbon deposition, electrochemical performance and mass change observed.
- Induction period prior to carbon deposition on SOFC anode identified.
- Carbon deposition on electrode surface confirmed with Raman spectroscopy.

GRAPHICAL ABSTRACT



ARTICLE INFO

Article history:

Received 30 August 2012

Received in revised form

5 December 2012

Accepted 5 February 2013

Available online 13 February 2013

Keywords:

Sensor

Coke

Nickel

Gallium phosphate

Raman spectroscopy

Microbalance

ABSTRACT

A novel bulk acoustic wave (BAW) microgravimetric sensor based on gallium orthophosphate is demonstrated that it is capable of operation at high temperature (up to 900 °C). The sensor is applied to the detection of carbon deposition onto electrodeposited nickel from dry methane at 600 °C and used as an analogue for studying the coking of solid oxide fuel cell (SOFC) anodes. The degradation of electrochemical performance due to deposition of carbon onto symmetrical SOFCs with nickel/gadolinium doped ceria electrodes is measured using electrochemical impedance spectroscopy (EIS). Direct correlation is observed between the frequency shift of the sensor and the change in resistance to charge transfer of the SOFC anode. An induction period (~2 h) following exposure to methane is observed where no significant carbon deposition occurs.

© 2013 Elsevier B.V. All rights reserved.

1. Introduction

Solid oxide fuel cells (SOFCs) offer the potential of cost effective, clean production of electrical power from natural gas and other hydrocarbons. Their high operating temperature allows the possibility of internal reforming of methane and other fuels directly on

* Corresponding author. Tel.: +44 (0)20 7679 3310.

E-mail address: d.brett@ucl.ac.uk (D.J.L. Brett).

URL: <http://www.ucl.ac.uk/centre-for-co2-technology>

the anode; this offers considerable advantages over low temperature fuel cells [1]. However, there are several major operational problems related to the internal reforming of hydrocarbons. One of them is the formation of coke deposits on the anode which can lead to catalyst deactivation, pore filling, loss of cell performance and impaired durability [1–4].

In SOFCs, carbon formation occurs when carbonaceous fuel with an insufficient steam-to-carbon ratio is exposed to the metallic component of the anode, which is typically nickel. This deposit blocks the reaction sites at the triple phase boundary (TPB) [5] and consequently access of hydrogen (or other fuels) is impaired and electrochemical performance degrades as a result [6].

The process of carbon deposition on SOFC anodes is complex and involves a range of mechanisms that are sensitive to operating parameters. The nature of the anode is also important and dependant on factors such as the catalyst-to-electrolyte ratio, porosity and particle size [7]. For example, smaller sized particles have been shown to be more resistant to coke formation [8].

The addition of steam to the hydrocarbon fuel is necessary for both the reforming and water gas shift reactions that take place at the anode. Indeed, steam is often added in excess of its stoichiometric amount to reduce the risk of carbon deposition. While an excess of steam is desirable for the mitigation of coke, it acts as a diluent, decreasing cell voltage and can lead to more rapid degradation of SOFC anodes [9]. In extreme cases, excess steam can lead to anode degradation by oxidising the Ni component of the catalyst, causing large volume expansions and reducing the active TPB length.

Above 450 °C carbon adsorbed on the nickel surface can diffuse to and then nucleate at available step and terrace sites [6,10]. These nucleation sites then allow for the growth of fibrous carbon structures. This reduces the number of active TPB sites by forcing the phases apart, blocking gas routes, increasing the mass transport resistance, reducing cell performance and potentially destroying the anode completely.

The type of carbon formed on SOFC anodes is dependent on temperature and time [11], with higher temperatures creating more tightly bound carbon formations, producing carbon nanotubes at 275–550 °C, char (soot) and amorphous carbon at 550–725 °C, and graphitic whisker carbon at >725 °C [6].

The current density at which the fuel cell operates also determines the rate and extent of carbon formation, as the flux of oxide ions through the electrolyte to the anode acts to suppress carbon formation by its oxidation to CO and CO₂. The presence of hydrogen can both reduce carbon through hydrogenation of the anode surface and increase carbon deposition; by reacting with adsorbed oxygen on the Ni, surfaces sites are freed up for the dissociative adsorption of CO, thus increasing the rate of coking [12]. A further complication arises when considering the spatial distribution of carbon deposition across the surface of SOFC anodes; temperature, fuel composition and local current density all affect this. Likewise, the kinetics of carbon deposition is a complex combination of factors such as electrode geometry, materials, steam-to-carbon ratio, reduction temperatures [13], current density, and residence time [14–16].

In order to understand the effect of operational variables on carbon deposition, and therefore minimise its formation, characterisation of the origin and rate of carbon formation is required. Current characterisation methods are applied *ex situ* and are too cumbersome and expensive to be integrated with technological fuel cells [17–19]. Hence, there is a need to study the carbon formation process *in situ* and in real time in order to understand the mechanisms and rate of reaction. Bulk acoustic wave (BAW) sensors are a potential technology for studying carbon deposition on catalyst surfaces. The most common BAW sensor is the quartz crystal microbalance (QCM) which is a mass sensing device with

nanogram resolution. The QCM uses the piezoelectric effect exhibited by suitably cut quartz, to relate oscillating frequency shift with mass deposition on to the crystal's surface using the Sauerbrey equation (Eq. (1)), where Δf is change in frequency, f_0 is original frequency, Δm is change in mass, A is area, ρ_q and μ_q is the density and shear modulus of quartz respectively [20].

$$\Delta f = \frac{-2f_0^2 \Delta m}{A \sqrt{\rho_q \mu_q}} \quad (1)$$

The QCM has been used in a wide range of applications but is limited to operation below 573 °C, above which the crystallographic structure changes and the quartz loses its piezoelectric properties [21]. Devices made using gallium orthophosphate (GaPO₄) offer greater high-temperature stability than conventional quartz crystals [22], presenting a strong candidate for resonator applications at high temperatures.

GaPO₄ crystals have been successfully used for *in situ* measurements of Al₂O₃ and TiO₂ film growth by atomic layer deposition at 450 °C [23]. Studies have also shown the possibility for gravimetric analysis using GaPO₄ resonators up to temperatures of 720 °C [24]. Previous work by the authors has demonstrated the use of the gallium orthophosphate microbalance (GCM) at temperatures relevant to solid oxide fuel cells and other high temperature heterogeneous catalyst applications [25]. The results presented here show how the GCM can be used alongside 'pellet' SOFCs to study carbon formation in a dry methane environment.

2. Experimental

In order to relate the results gathered using the GCM to fuel cell coking, a symmetrical pellet SOFC was operated simultaneously, experiencing the same gas/temperature environments. The SOFC was subjected to EIS measurements approximately every 15 min (~10 min scan time, 5 min hold) whilst the GCM frequency was measured every 10 s continuously. The GCM's temperature coefficient of frequency depends on the cut of the crystal; previous work has shown the Ni–GCM to be least sensitive to temperature in the range of 600 °C [25]. At 600 °C, temperature changes of ±10 °C caused by altering gas between N₂, H₂ and CH₄ lead to a frequency change of ±7 Hz, which corresponds to a mass change of ±0.03 µg.

The GCM used in this study is the same as that reported previously [25], consisting of gallium orthophosphate crystals (y-11.1° cut, R-30, Q-factor = 70,000, resonant frequency = 5.8 ± 0.1 MHz, sensitivity ~0.3 ng Hz⁻¹) with a double anchor metallization (curvature = 2 dioptre) on one side and full metallization (flat) on the other. On both sides the electrode is platinum (~200 nm) with a titanium adhesion underlayer (~20 nm). These devices are commercially available from Piezocryst Advanced Sensorics GmbH (Graz, Austria).

Using a specifically designed holder the Pt electrodes on the crystals are nickel plated at the centre to provide the catalytic surface required. A Watts bath was used consisting of a solution of 0.647 M H₃BO₃, 0.285 M NiSO₄·6H₂O and 0.047 M NiCl₂·6H₂O [26,27]. The solution was bubbled through with nitrogen to rid the chamber of oxygen as well as to remove H₂ bubbles formed at the surface. A Ni counter electrode was used together with a Hg/Hg₂Cl₂ (SCE) reference electrode. An Autolab PGSTAT302N (Metrohm Autolab, Netherlands) potentiostat, was used to perform Ni plating at -1.1 V vs. SCE for 900 s. The GCM calculated mass change associated with the electrodeposited Ni layer corresponds to a thickness of ~3 µm; SEM and EDS analysis confirmed a full and even nickel coating of Ni on Pt.

A symmetrical SOFC (i.e., anode electrodes on both sides of the electrolyte and operated in a common gas environment) was used

in order to focus on the effect of fuel gas on the anode without the need to deconvolute the effect of the cathode from the overall electrochemical response. The SOFC was produced using yttria-stabilised zirconia (YSZ) electrolytes (20 mm diameter and 250–300 μm thick) from [fuelcellmaterials.com](#). Ceramic-metal (cermet) electrodes based on a mixture of nickel and gadolinium doped ceria (Ni–CGO) were prepared using 40 wt.% CGO-10, (Rhodia) and 60 eq. wt.% Ni in the form of green NiO (Alfa Aesar) mixed with additives such as binder, dispersant, plasticiser and solvent. The anode material was painted by hand onto the YSZ substrate and sintered at 1300 °C for 2 h in air [28]. Cells were reduced for 3 h in dry hydrogen environment and had a thickness of ~11 μm after reduction.

Testing of the pellet SOFCs and GCM required a holder that could provide good electrical connections, even and stable compression across the temperature range, and reactant access to the electrodes. In addition, the ability to replace the sample/sensor rapidly without damage to the device or holder is desirable. Fig. 1 shows an exploded view of the holder, illustrating how the SOFC pellet is closely positioned alongside the GCM, ensuring well matched gas and temperature conditions (a K-type thermocouple is integrated within the holder). The holder is composed of three central body parts integrating the GCM and SOFC with two ‘push fit’ end pieces that fit around the conical shapes that the central sections form when combined together, thereby providing the necessary compression during experimentation.

All of the body parts are made from machinable ceramic (pyrophyllite from Ceramic Substrates and Components Ltd, UK) formed using a desktop CNC (Computer Numerical Control) machine (Roland MDX-40). Electrical connections are made to the SOFC and GCM using platinum painted tracks (4082 Pt conductor, Ferro, UK) on the ceramic pieces. Platinum mesh (plain weave mesh, 99.9% purity, wire diameter 0.06 mm, open area 65%, Goodfellow, UK) is sandwiched between the platinum painted tracks and SOFC electrodes to provide good electrical connection.

The holder was positioned within a sealed quartz tube ($\phi = 6.6 \text{ cm}$, $l = 80 \text{ cm}$, volume ~2.7 L) in a horizontal split tube furnace (Lenton, UK) in order to accurately control the temperature and gaseous environment of the combined SOFC and GCM. The gas environment was controlled using calibrated mass flow controllers (EL-FLOW, Bronkhorst, UK) using flow rates of 100 $\text{cm}^3 \text{ min}^{-1}$. The oscillation frequency of the GCM was measured using a Q-pod Quartz Crystal Monitor (Inficon, UK) interfaced to a PC.

Electrochemical impedance spectroscopy (EIS) was performed on symmetrical SOFCs using an Iviumstat potentiostat (Alvatek Ltd.,

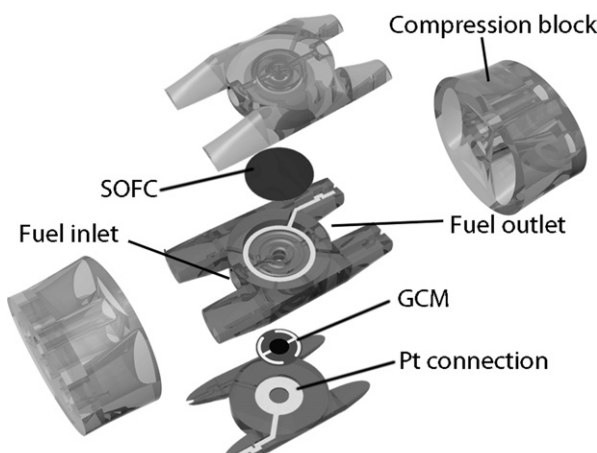


Fig. 1. Exploded view of the components of the all-ceramic combined SOFC/GCM push fit holder.

UK). Impedance scans were run over a frequency range of 100 kHz–0.1 Hz with a voltage amplitude of 10 mV. The impedance responses were fitted to the equivalent circuit shown in Fig. 2. Since the SOFC is a symmetrical cell, the two RC combinations associated with the respective electrodes (Fig. 2(a)) are theoretically the same and can be combined (Fig. 2(b)). Symmetrical cell operation means that there is no DC polarisation of the cell, mass transport limitation is therefore not expected to be as significant as the kinetic limitation. However, since we are dealing with a porous structure, some mass transport resistance is likely to be present. Since there is no evidence of separate electro-kinetic and mass transport features (i.e., there is only one arc in the Nyquist plot) the arc is generically described as the electrode resistance to charge transfer (R_{ct}).

Since the SOFC electrodes are highly porous and have a distributed electrochemical performance, a purely capacitive equivalent circuit component is not appropriate. Therefore a constant phase element (CPE) component is used. This accounts for the depressed semi-circular arcs observed in the Nyquist plots.

Raman spectroscopy measurements were taken using a Renishaw RM-2000 CCD spectrometer. Spectra were obtained using a high numerical aperture $\times 50$ short working distance objective which allowed the laser to be focused on to the samples surface to a spot size of approximately 1.5 μm . Measurements were taken using a 514 nm argon ion laser with approximately 1 mW of laser power at the focal point and an integration time of 10 s was used.

3. Results and discussion

Although other chemicals and fuels have a greater propensity for coke formation (ethylene and many aromatic compounds for example), methane is the most common hydrocarbon fuel used in SOFCs and was thus used here to see if the GCM could detect coke formation in parallel with SOFC operation.

3.1. Electrochemical impedance spectroscopy of fuel cell anode

Fig. 3 shows five examples of measured EIS results (Nyquist plots). The graph shows a typical electrode/electrolyte response associated with symmetrical SOFCs composed of a single depressed semicircle, in accord with the equivalent circuit shown in Fig. 2(b) [29]. The location at which the high frequency impedance intercepts the real impedance axis provides the series resistance, $R_s(Z_{\text{HF}})$. This is associated with the combined Ohmic resistance associated with the electrolyte, electrodes, contact resistance between electrode and current collector and the uncompensated lead resistance. Since these measurements were performed at constant temperature, the resistance of the electrolyte is neither expected to change, nor is the uncompensated lead resistance. Therefore, any change in this parameter can be reasonably associated with the resistance of the anodes and electrode/current collector interface.

The low frequency intercept with the real axis (Z_{LF}) represents the combination of series and charge transfer resistance, $R_s + R_{\text{ct}}$. In Fig. 3, the ‘4 h’ plot has been labelled to illustrate these intersections. As operation is carried out on a symmetrical cell, R_{ct} represents a combination of both Ni-CGO anodes and must therefore be halved to give a true reading for a single anode. All R_{ct} values that follow are given for a single electrode.

3.2. Comparison of crystal frequency response to anode impedance

By plotting both the R_s and R_{ct} values over time it is possible to see the increase in resistance of the electrodes (assuming that there is no change in the resistance of the electrolyte) caused by degradation from coking (Fig. 4). Also shown is the frequency response of the GCM operating simultaneously with the SOFC. The GCM

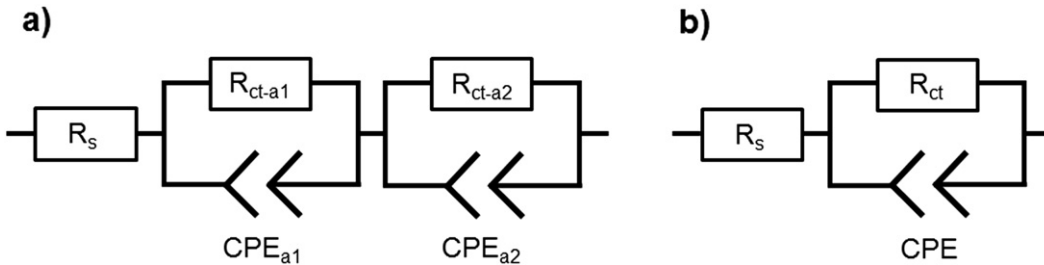


Fig. 2. (a) SOFC equivalent circuit, where R_s is the series resistance composed of electrolyte, electrodes, interconnects and uncompensated lead resistance, R_{ct} is the resistance to charge transfer and CPE is the constant phase element associated with the capacitive nature of the electrode/electrolyte interface; (b) equivalent circuit combining the R_{ct} /CPE parallel combination for each 'identical' electrode.

demonstrates a decrease in frequency (gain in mass) associated with exposure to dry methane that correlates with the change in charge transfer resistance, R_{ct} .

The EIS and GCM profile in Fig. 4(a) can be notionally segmented into three regions: (i) purge and induction, (ii) deposition, and (iii) bulk deposition. During the start of the first region of (40 min) there is an initial small increase in R_{ct} whilst R_s remains relatively level, this is associated with switching hydrogen feed to methane [30–32]. The R_{ct} is increased due to the more sluggish CH₄ decomposition/oxidation compared to hydrogen. There will also be a lower partial pressure of hydrogen in the reactor. With a flow rate of 100 cm³ min⁻¹, purging of the 2737 cm³ system is associated with the initial increase in R_{ct} that occurs over a period of 40 min.

From a thermodynamic perspective, carbon deposition becomes more likely as the fraction of methane increases. For the Boudouard reaction, it is has been reported that a certain excess of CH₄ is required to initiate the reaction [33]. During region (i) the limited increase in R_{ct} and the slight frequency decrease of the GCM implies that there is no sign of significant carbon deposition. Reports have described an induction period prior to multilayer carbon deposition for various carbonations gas environments onto nickel [33–36]. In previous studies using thermogravimetric analysis (TGA), it has been proposed that during the induction period carbon is 'dissolved' into the metal before it can begin to grow from the surface at facets and step sites [10,37–39]. Gardner and Bartholomew [40] reported a similar transient to that in Fig. 4(a) from a CO containing gas mixture onto Ni.

Measured in pure, dry hydrogen prior to the introduction of the methane, the symmetrical cell has an inherent R_{ct} degradation rate of 1.1 Ω cm² h⁻¹, this is higher than previous studies using the same anode material [29]; however, degradation has been shown to be higher in dry than 'wet' hydrogen [9]. The inherent degradation can be attributed to sintering of the cermet microstructure with loss of three phase boundary reaction sites. The series resistance, R_s , shows no discernible change during operation on pure hydrogen, which suggests the interface (contact resistance) between the Pt current collector and the electrodes is stable.

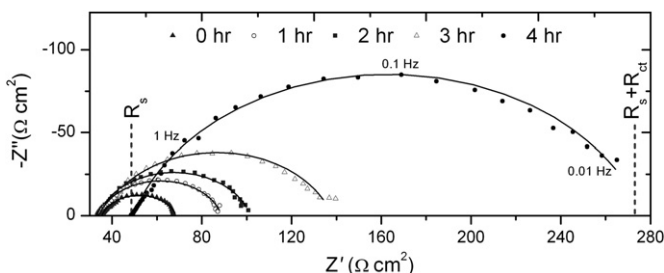


Fig. 3. Fitted EIS scans of the symmetrical pellet cell at 600 °C in CH₄ (100 sccm) evolving with time (1 h between scans).

When assuming a linear fit for Fig. 4(a) from 40 min to 2 h an R_{ct} degradation rate of 6.5 Ω cm² h⁻¹ is observed. This is higher than the pure hydrogen degradation rate and associated with the effect on the anode due to 'induction period' processes. During this period there is no significant change in either the R_s or GCM response.

The second region, (ii), occurs between ~2 and 6 h and shows the period in which carbon deposition occurs. This is referred to in the literature for carbon deposition onto Ni catalysts as the steady state phase [34]. Linearising this period gives an R_{ct} increase of 49.5 Ω cm² h⁻¹ per anode. There is an increase in R_s during this period at a rate of 12.2 Ω cm² h⁻¹, which is assumed to be due to a decrease in contact resistance between the electrode and current collector due to carbon deposition or change in the DC conductivity of the electrode. The GCM during this period demonstrates a frequency shift of 2990 Hz; which, using the Sauerbrey equation, relates to a 2.4 μg h⁻¹ mass change, assuming a linear increase.

Region (iii) is associated with a rapid increase in R_s and at 7.32 h the SOFC fails. This suggests that carbon deposition either leads to detachment/blockage of the current collector from the electrode or delamination of the anode material away from the electrolyte, the prelude to each of these catastrophic failures is likely to be associated with a rapid increase in series resistance as observed.

The Sauerbrey equation offers a quantitative relationship between a GCM's frequency shift and mass deposition. While this equation is known to be accurate for mass measurements of many systems (the Ni electrodeposition used to coat the Pt electrodes in

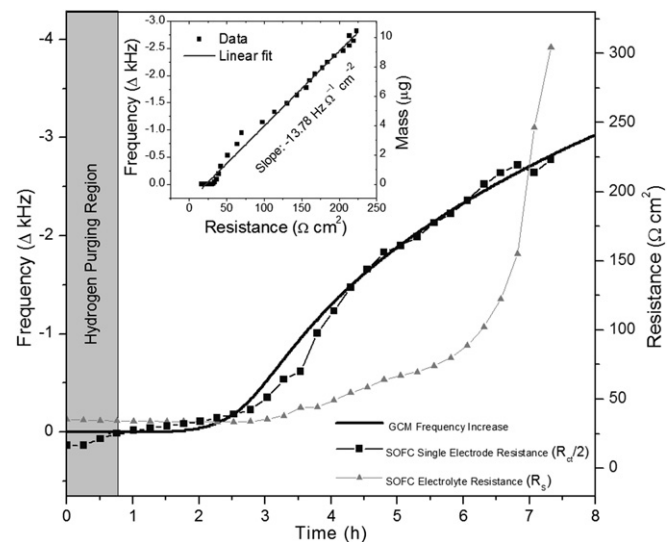


Fig. 4. Comparison of GCM frequency (left axis) and resistances of symmetrical pellet SOFC (right axis) at 600 °C when introduced to CH₄ (100 sccm), GCM scanned continually and EIS of SOFC at 15 min intervals. Graph inset shows the correlation between mass deposited on the GCM (inferred from the Sauerbrey equation) and resistance related to charge transfer of a single SOFC anode with a fit as a guide to the eye.

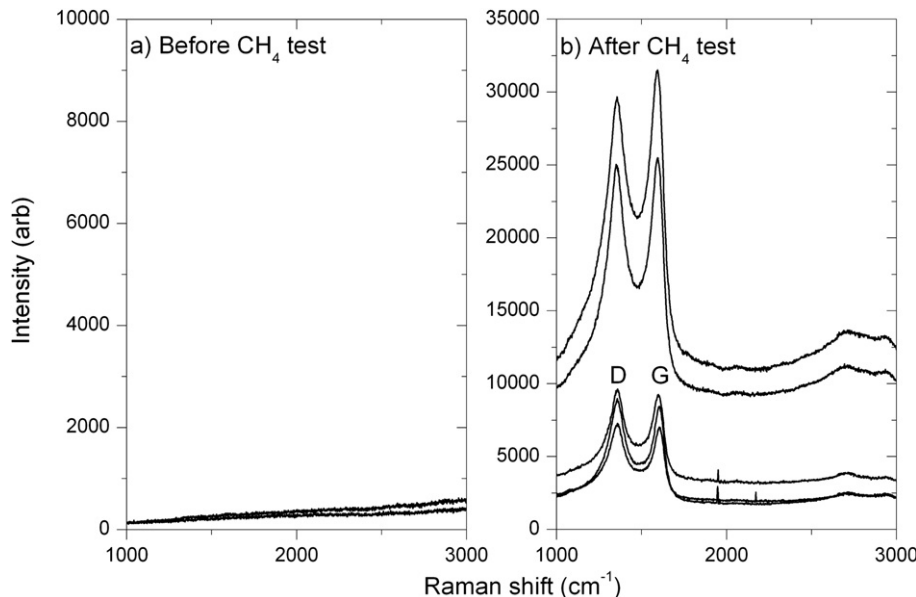


Fig. 5. Raman spectroscopy of Ni–GCM before and after CH_4 environment taken at random points on electrode.

this study, for example), it is subject to a number of constraints. These are primarily that the deposition layer must be homogeneous and rigid. The nature of carbon deposition onto the GCM electro-deposited Ni layer means that the Sauerbrey equation cannot be strictly applied and therefore any mass changes implied cannot be quantitatively relied upon. However, the qualitative relative change and transition dynamics are reliable and valuable diagnostics. As can be seen in the graph inset in Fig. 4, there is excellent correlation of R_{ct} with the GCM response in terms of both frequency and calculated mass change. During this time the calculated GCM mass change (using the Sauerbrey equation) of $10.4 \mu\text{g}$ compares to a measured mass change experienced by the SOFC of $478 \mu\text{g}$ (weighed ex-situ post-test). The large difference in measured mass between these systems is to be expected due to the differences in surface area and nature of the smooth electroplated Ni layer compared to the SOFC cermet anode. Using the SOFC measured weight, a mass resistance relationship of $0.1 \Omega \text{ cm}^2 \mu\text{g}^{-1}$ results (when the anode natural degradation of $1.1 \Omega \text{ cm}^2 \text{ h}^{-1}$ is removed).

3.3. Raman spectroscopy of anode and GCM surfaces

Raman spectroscopy is a powerful and convenient method for the detection and characterisation of carbon on a wide variety of surfaces [41–43]. Graphitic materials produce a distinctive Raman fingerprint which usually includes the D and G peaks located at approximately 1350 cm^{-1} and 1590 cm^{-1} respectively. The D peak is related to defects within the graphitic structure such as grain boundaries and point defects while the G peak is directly related to the graphitic structure. The relative intensity of these two peaks as well as their widths and positions allows for detailed information regarding the physical nature of the probed carbon deposits to be ascertained. For example, the presence of an intense D peak coupled with broad features is indicative of amorphous carbon where the defect density is relatively high. On the other hand, more graphitic carbon would be characterised by a small D to G peak intensity and much sharper features. This has been demonstrated in a number of publications [18,44].

Raman experiments were carried out *ex situ* at room temperature for samples previously exposed to CH_4 . The samples were purged with nitrogen then cooled at 5°C min^{-1} from the operating

temperature of the experiment. Fig. 5 shows the Raman spectra for the GCM before and after exposure to a CH_4 environment, taken at random points on the electrode.

The GCM surface shows the characteristic features (D and G peaks) and is considered clear evidence of carbon deposition. The Ni–GCM surface can be said to be amorphous in nature due to the broad features observed and more intense D peak relative to the G peak (average D/G ratio of the 5 spectra that we show in the paper is 1.15 ± 0.5). The large difference in intensity between scans indicates a significant distribution of carbon on the surface and the non-uniform D/G intensity ratio suggests a slight variation in the type of carbon that is produced. The amorphous nature agrees with the type of carbon that should be formed at these temperatures on SOFCs [6].

4. Conclusions

The GCM is a promising new sensor technology for studying coke formation on heterogeneous catalyst surfaces. Operation of the GCM alongside a symmetrical SOFC pellet cell during exposure to dry CH_4 at 600°C shows a close correlation between the frequency shift and resistance to charge transfer of the SOFC determined using electrochemical impedance spectroscopy. With further study, the $R_{\text{ct}}/\Delta f$ relationship may prove to be a useful diagnostic to help improve our understanding of carbon formation and other surface processes that occur at high temperature. However, it is clear from this study that the GCM is a promising sensor for use in technological SOFCs and fuel processors to incorporate into control systems to monitor carbon deposition.

An induction period of several hours is identified for coke formation on SOFCs, this is in accord with the known phenomenon on nickel based catalysts. The fact that there is a significant period between exposure to methane and the onset of the coking may have implications for SOFC operation so as to avoid this degradation process.

Acknowledgements

The authors would like to acknowledge the EPSRC project EP/I037024/1 for supporting the work of JM, the EPSRC Supergen Fuel Cells program (EP/G030995/1) for funding the research of DB, NB

and TM, the EPSRC Platform Grant for Functional Magnetic Materials (EP/E016243/1) for RCM and the National Physical Laboratory for the on-going support of this project.

References

- [1] S.H. Clarke, et al., *Catal. Today* 38 (4) (1997) 411–423.
- [2] T. Kim, et al., *J. Power Sources* 155 (2) (2006) 231–238.
- [3] C.M. Finnerty, et al., *Catal. Today* 46 (2–3) (1998) 137–145.
- [4] Y. Lin, et al., *Solid State Ionics* 176 (23–24) (2005) 1827–1835.
- [5] N.P. Brandon, D.J. Brett, *Philos. Trans. R. Soc. A* 364 (1838) (2006) 147–159.
- [6] G.J. Offer, et al., *J. Am. Ceram. Soc.* 92 (4) (2009) 763–780.
- [7] E. Ivers-Tiffée, et al., Methane Reforming Kinetics, Carbon Deposition, and Redox Durability of Ni/8 Yttria-stabilized Zirconia (YSZ) Anodes, in: *Handbook of Fuel Cells*, John Wiley & Sons, Ltd, 2010.
- [8] K.O. Christensen, et al., *Appl. Catal. A* 314 (1) (2006) 9–22.
- [9] P. Kim, D.J.L. Brett, N.P. Brandon, *J. Power Sources* 189 (2) (2009) 1060–1065.
- [10] H.S. Bengaard, et al., *J. Catal.* 209 (2) (2002) 365–384.
- [11] I. Alstrup, et al., *Mater. Corros.* 49 (5) (1998) 367–372.
- [12] G.J. Offer, N.P. Brandon, *Chem. Eng. Sci.* 64 (10) (2009) 2291–2300.
- [13] C. Mallón, K. Kendall, *J. Power Sources* 145 (2) (2005) 154–160.
- [14] J.W. Snoeck, G.F. Froment, M. Fowles, *J. Catal.* 169 (1) (1997) 250–262.
- [15] A.K. Avetisov, et al., *J. Mol. Catal. A Chem.* 315 (2) (2010) 155–162.
- [16] J. Zhang, D.J. Young, *Corros. Sci.* 49 (3) (2007) 1496–1512.
- [17] C.A. Querini, S.C. Fung, *Catal. Today* 37 (3) (1997) 277–283.
- [18] M.B. Pomfret, J.C. Owirutsky, R.A. Walker, *J. Phys. Chem. B* 110 (35) (2006) 17305–17308.
- [19] H. He, J.M. Hill, *Appl. Catal. A* 317 (2) (2007) 284–292.
- [20] G.Z. Sauerbrey, *J. Phys.* 155 (1959) 206–212.
- [21] F. Krispel, et al., Properties and Applications of Singly Rotated GaPO₄ Resonators, in: *Proceedings of the 2003 IEEE International Frequency Control Conference* (2003).
- [22] H. Thanner, et al., *Vacuum* 67 (3–4) (2002) 687–691.
- [23] J.W. Elam, M.J. Pellin, *Anal. Chem.* 77 (11) (2005) 3531–3535.
- [24] H. Thanner, et al., *J. Therm. Anal. Calorim.* 71 (1) (2003) 53–59.
- [25] J. Millichamp, et al., *Ind. Eng. Chem. Res.* 50 (13) (2011) 8371–8375.
- [26] T. Mimani, S.M. Mayanna, N. Munichandraiah, *J. Appl. Electrochem.* 23 (4) (1993) 339–345.
- [27] J.P.G. Farr, A.J.S. McNeil, *Surf. Coat. Technol.* 3 (5–6) (1975) 399–415.
- [28] S. Baron, et al., *J. Power Sources* 126 (1) (2004) 58–66.
- [29] P. Lohsoontorn, D.J.L. Brett, N.P. Brandon, *J. Power Sources* 183 (1) (2008) 232–239.
- [30] E.P. Murray, T. Tsai, S.A. Barnett, *Nature* 400 (6745) (1999) 649–651.
- [31] J.H. Koh, et al., *Solid State Ionics* 149 (3–4) (2002) 157–166.
- [32] S. Li, et al., *J. Solid State Electrochem.* 11 (1) (2007) 59–64.
- [33] J.R. Rostrup-Nielsen, *J. Catal.* 27 (3) (1972) 343–356.
- [34] L.S. Lobo, D.L. Trimm, *J. Catal.* 29 (1) (1973) 15–19.
- [35] J.R. Rostrup-Nielsen, D.L. Trimm, *J. Catal.* 48 (1–3) (1977) 155–165.
- [36] Q. Zhuang, Y. Qin, L. Chang, *Appl. Catal.* 70 (1) (1991) 1–8.
- [37] T. Borowiecki, A. Machocki, J. Ryczkowski, Induction Period of Coking in the Steam Reforming of Hydrocarbons, in: B. D (Ed.), *Studies in Surface Science and Catalysis Catalyst Deactivation 1994 Proceedings of the 6th International Symposium*, Elsevier, 1994, pp. 537–542.
- [38] R.T. Yang, J.P. Chen, *J. Catal.* 115 (1) (1989) 52–64.
- [39] A.J.H.M. Kock, et al., *J. Catal.* 96 (2) (1985) 468–480.
- [40] D.C. Gardner, C.H. Bartholomew, *Ind. Eng. Chem. Prod. Res. Dev.* 20 (1) (1981) 80–87.
- [41] R.C. Maher, et al., *J. Am. Chem. Soc.* 112 (7) (2008) 1497–1501.
- [42] T.V. Reshetenko, et al., *Carbon* 41 (8) (2003) 1605–1615.
- [43] S.K. Doorn, et al., *J. Phys. Chem. B* 109 (9) (2005) 3751–3758.
- [44] C. Su, et al., *J. Power Sources* 196 (4) (2011) 1967–1974.